ELSEVIER

Journal of Molecular Catalysis A: Chemical 131 (1998) 285–299

JOURNAL OF MOLECULAR CATALYSIS A: CHEMICAL

Controlling surface reactivities of transition metals by carbide formation

Jingguang G. Chen [a,*], Bernd Frühberger [a,1], Joseph Eng Jr. [b,2], Brian E. Bent [b]

[a] *Corporate Research Laboratories, Exxon Research and Engineering, Annandale, NJ 08801, USA*
[b] *Department of Chemistry, Columbia University, New York, NY 10027, USA*

Received 6 June 1997; accepted 27 August 1997

Abstract

The surface reactivities of transition metals, including the Groups 4–6 early transition metals as well as the late transition metals of the 3d series, can often be modified by the formation of a carbide overlayer. More importantly, the reactivities of carbide-modified surfaces frequently demonstrate strong similarities to those of the Pt-group (Pt, Pd, Ir, Rh, Ru and Os) metals. In this paper, we will summarize our recent surface science investigations of the electronic, structural, and catalytic properties of well-characterized model carbide systems. Using several characteristic surface probing reactions, we will provide experimental evidence for the similar reactivities of the carbide-modified surfaces and the Pt-group metals. We will also discuss the underlying structural and electronic properties that are controlling the reactivities of the carbide-modified surfaces, such as the binding sites and chemical nature of the carbon atoms, the ionicity of the metal–carbon bonds, and the band structure of the transition metal carbides. We will also show examples of experimental attempts to correlate findings from the single crystal model carbide systems to amorphous powder carbide catalysts. © 1998 Elsevier Science B.V.

Keywords: Surface reactivities; Transition metals; Carbide formation

1. Introduction

Transition metal carbides are formed when carbon atoms, produced by decomposition of hydrocarbons or other carbon-containing molecules, are incorporated into the metal interstitial sites. As shown in Table 1, stable carbides are typically found for 3d metals, and for 4d and 5d metals on the left-hand side of the Periodic Table, mainly Groups 3–6 metals [1–4]. In general, transition metal carbides are characterized by unique physical and chemical properties, which combine the characteristic properties of three different classes of materials: covalent solids, ionic crystals and transition metals [1–4]. For example, they demonstrate the extreme hardness and brittleness of covalent solids; they possess the high melting temperature and simple crystal structures typical of ionic crystals; and they have electronic and magnetic properties that are similar to transition metals.

Because of their refractory and conducting nature, one of the practical applications of tran-

* Corresponding author.
[1] Current address: The BOC Group, Murray Hill, NJ 07974.
[2] Current address: Corporate Research Laboratories, Exxon Research and Engineering, Annandale, NJ 08801.

1381-1169/98/$19.00 © 1998 Elsevier Science B.V. All rights reserved.
PII S1381-1169(97)00271-9

Table 1
Examples of stable transition metal carbides

Chemical groups						
4	5	6	7	8	9	10
TiC	VC	Cr_3C_2	Mn_3C	Fe_3C	Co_3C	Ni_3C
ZrC	NbC	Mo_2C				
HfC	TaC	WC; W_2C				

sition metal carbides is in materials science [1–6]. In addition, these carbide materials also often demonstrate unique catalytic properties, which will be the subject of this review. It has been shown in the catalysis literature that transition metal carbides often possess catalytic advantages over their parent metals in activity, selectivity and resistance to poisoning [2–4]. Most of these catalytic studies were inspired by the landmark paper by Levy and Boudart [7], who demonstrated that tungsten carbides displayed Pt-like properties in several catalytic reactions. The catalytic properties of transition metal carbides have been the subject of several recent reviews [2–4]. In general, transition metal carbides have been demonstrated to have excellent catalytic activities in a variety of reactions [2–4], including hydrogenolysis, hydrogenation, dehydrogenation, isomerization, methanation, hydrodesulfurization (HDS) and hydrodenitrogenation (HDN). One of the primary motivations in the catalytic applications of transition carbides has been to use them as cheaper alternative catalysts to replace the more expensive Pt-group metals (Pt, Pd, Ir, Rh, Ru and Os). For example, for hydrogenation and hydrogenolysis reactions, several transition metal carbides demonstrate catalytic activities that are similar to or greater than those of Pt-group metals [2–4]. Experimental results also indicated that carbide catalysts can be potentially more desirable catalysts than the Pt-group metals for certain types of reactions. For example, carbide catalysts often showed unique catalytic pathways, leading to more desirable product selectivities [2–4,8]. Another potential catalytic advantage of carbide catalysts is that they often show higher sulfur [2–4,9] and nitrogen tolerance than the Pt-group metals [2–4,10].

The unique physical, chemical and catalytic properties of transition metal carbides have inspired many surface science studies [5,6], using well-characterized carbide surfaces as model systems. The carbide surfaces can be prepared either by in situ cleaning of bulk single crystal carbides [5] or by the formation of a thin carbide overlayer on the single crystal surfaces of the parent transition metals [6]. For the investigation of catalytic properties, choosing carbide overlayers as model systems has several advantages over the bulk carbide single crystals [6]: (1) It allows one to compare directly the chemical reactivities of the carbide surfaces with those of the parent metal surfaces; (2) it enables one to vary the carbon/metal stoichiometries; and (3) it allows one, in some cases, to control the binding sites of the carbon atoms. These aspects will be discussed in detail in this manuscript.

The majority of the surface science studies of the reactivities of carbide overlayers has been concentrated on early transition metal surfaces, particularly on vanadium [11–14] [3], molybdenum [15–30] and tungsten [31–42] single crystal surfaces. By using simple inorganic and organic molecules as probing molecules, these studies indicated that the reactivities of transition metal surfaces could be substantially modified by the formation of carbide. In the past few years we have investigated the electronic, structural and catalytic properties of carbide overlayers on several closed-packed transition metal surfaces, including V(110) [11–14] [3], Mo(110) [24–30], Ti(0001), Fe(110) and Ni(111). In these studies, we employed a variety of surface science techniques, including high-resolution electron energy loss spectroscopy (HREELS), near-edge X-ray absorption fine structure (NEXAFS), X-ray photoelectron spectroscopy (XPS), Auger electron spectroscopy (AES), low energy elec-

[3] J.G. Chen, B. Frühberger, M.D. Weisel, J.E. Baumgartner, B.D. DeVries, in Ref. [3], p. 439.

tron diffraction (LEED) and temperature programmed desorption (TPD). Our primary interest has been to correlate the unique chemical properties of the carbide overlayers to their underlying electronic and structural properties.

The rest of this manuscript is organized as follows: In Section 2, we will describe very briefly the preparation and characterization of carbide overlayers. In Section 3, we will demonstrate the conversion of surface reactivities of an early transition metal, Mo(110), to those of Pt-group metals via the formation of molybdenum carbide. We will discuss three surface reactions that can be used to probe the characteristic reactivities of carbide-modified surfaces: the formation of ethylidyne (CCH_3) from the partial decomposition of ethylene, the production of surface 2-butyne from the selective activation of α- and β-CH bonds of *cis*- and *trans*-2-butenes, and the evolution of gas phase benzene from the dehydrogenation of cyclohexene. In Section 4, will discuss the underlying electronic and structural factors that are controlling the reactivities of carbide overlayers. These factors include the binding sites of carbon atoms (e.g., surface vs. interstitial sites), the chemical nature of carbon atoms (e.g., carbidic vs. graphitic forms), and the electronic properties of the carbide overlayer, such as the ionicity of metal–carbon bonds and the p-projected density of states. In Section 5, we will briefly address the correlation between well-characterized single crystal carbide overlayers and amorphous powder carbide catalysts using NEXAFS. Finally, in Section 6, we will provide concluding remarks, as well as potential research opportunities, regarding the catalytic properties of transition metal carbides.

2. Preparation of transition metal carbide overlayers

Carbide overlayers on transition metal surfaces can be produced by the thermal cracking of unsaturated hydrocarbon molecules such as ethylene. The most efficient temperature for the thermal cracking varies from metal to metal, although annealing to temperatures above 600 K is often required to obtain sharp LEED patterns. The formation of well-characterized carbide overlayers is most commonly verified using XPS, AES and LEED. A summary of various carbide-modified transition metal surfaces, including the LEED patterns and the corresponding carbon/metal stoichiometries, can be found in a recent review [6].

Fig. 1 shows an example of utilizing AES to follow the preparation of a carbide overlayer on a Mo(110) surface by exposing the clean Mo(110) surface to ethylene at 600 K [24]. At this temperature ethylene undergoes complete

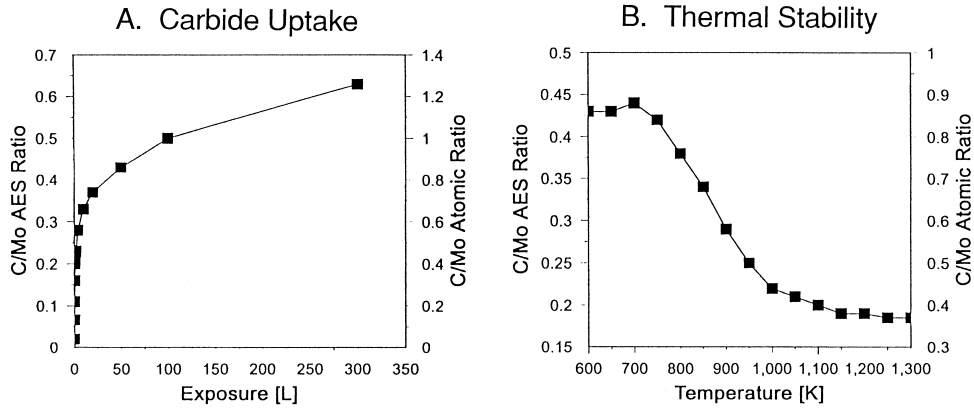

Fig. 1. AES measurements following the uptake (A) and annealing (B) of carbide overlayers on a Mo(110) surface.

decomposition on the Mo(110) surface to produce atomic carbon and hydrogen, with the latter recombining to desorb as gas phase H_2. The complete decomposition of ethylene on Mo(110) was verified using HREELS, which confirmed the absence of any vibrational modes that might be related to surface C_xH_y fragments [24]. As shown in Fig. 1A, the carbon uptake is monitored by measuring the AES peak-to-peak intensity ratio of the C(KLL)/Mo(MNN) Auger transitions as a function of ethylene exposure at 600 K. Also shown in Fig. 1A are the carbon/molybdenum atomic ratios, which are estimated by using the relative AES sensitivity factors for the respective Auger transitions [24]. The C(272 eV) Auger signal displayed the three-lobed lineshape characteristic for carbidic carbon species throughout the entire range of exposures, demonstrating the absence of any graphitic carbon on the carbide overlayers. Furthermore, the corresponding LEED studies showed an increase in the diffuse background intensity with increasing exposure to ethylene, indicating the absence of any ordering of the carbide overlayer at 600 K.

Fig. 1B shows the thermal stability of a molybdenum carbide overlayer [24], which was prepared by exposing Mo(110) to 100 L (1 L = 10^{-6} Torr s) ethylene at 600 K and was characterized by an initial C(KLL)/Mo(MNN) Auger ratio of $\sim$0.43. There are distinct temperature regimes in Fig. 1B: the C/Mo ratio remains relatively constant between 600–700 K; it shows a continuous decrease between 700–1150 K; it remains constant again at 1150–1300 K. In addition, after annealing the carbide overlayer to above 1150 K, the surface displayed a well defined p(4 × 4) LEED pattern. No desorption of any carbon containing species was detected in TPD studies above 600 K, suggesting that the decrease in the C Auger signal is related to an inward diffusion of carbon into the bulk of the Mo(110) sample above $\sim$700 K. Further NEXAFS and XPS [25] of the same C/Mo(110) overlayers confirmed a thermally-induced diffusion of surface carbon atoms into the interstitial sites after heating to above 1150 K. As will be demonstrated later in Section 4.1, the chemical reactivities of the surface and interstitial carbide overlayers are drastically different.

3. Characteristic probing reactions on carbide-modified surfaces

Previous surface science studies, particularly those on carbide-modified V(110) [11–14] [3] and Mo(110) [24–30] surfaces, have provided conclusive evidence that the reactivities of early transition metals can be converted to those of Pt-group metals via the formation of surface carbide. Various simple molecules have been used to probe the reactivities of carbide-modified surfaces [6], including simple inorganic molecules such as CO and HCN, and organic molecules such as alkanes, alkenes, aromatics, oxygenates, and thiophenes. Among them, the most characteristic and simple probing reactions to identify the Pt-like surface reactivities are the decomposition of ethylene, *cis*- and *trans*-2-butenes, and cyclohexene on the carbide-modified surfaces. In this section, we will compare the decomposition mechanisms of these probing molecules on Mo(110), p(4 × 4)-C/Mo(110), and Pt(111) to demonstrate the similar surface reactivities between carbide-modified Mo(110) and Pt-group metal surfaces.

3.1. Formation of ethylidyne from ethylene decomposition

One of the main advantages of using ethylene as a probing molecule is that the adsorption and decomposition of ethylene on transition metal surfaces have been investigated extensively in both experimental and theoretical studies. The interaction of ethylene with transition metals is usually described in terms of the Dewar–Chatt–Duncanson mechanism, which involves primarily the donation-back-donation of π-electrons of ethylene and d-electrons of metals [43]. In this mechanism, electrons in the highest filled

π-orbital of ethylene are partially donated to an empty σ-orbital of the metal atom. Such a donation weakens the π-bond of ethylene and lowers the energy level of the lowest-lying antibonding π^*-orbital, which in turn allows a more efficient back-donation of electrons from the metal atom, further weakening the C=C bond. Because the degree of π–d interaction depends strongly on the characteristics of the metal d-orbitals, one would expect the interaction of ethylene with metals to be different from one chemical group of metals to another. Indeed, both theoretical calculations [43] and experimental studies [44–46] have demonstrated that the reaction pathway of ethylene is often distinctly different for transition metals from the left hand to the right hand side of the Periodic Table, with early transition metals interacting more strongly with ethylene. For example, early transition metals are generally found to be highly reactive, leading to the formation of deeply dehydrogenated products, C_2H_x ($x \leq 2$), with both carbon atoms bonding to the surface. These intermediates undergo further thermal decomposition to produce atomic carbon and hydrogen. In contrast, the interaction of ethylene with late transition metals, particularly the Pt-group metals, generally occurs via different mechanisms. It is now well documented that the reaction of ethylene with the close-packed faces of Pt [47–49] and other Pt-group metals [50–53] (Pd, Ir, Rh, and Ru) is characterized by the formation of an ethylidyne (CCH_3) surface intermediate; this intermediate can be readily detected using surface vibrational spectroscopies such as HREELS.

Figs. 2 and 3 show a comparison of HREELS results of different reaction pathways of ethylene on clean Mo(110) and p(4 × 4)-C/Mo(110) surfaces [26]. As shown in Fig. 2, the HREELS spectrum, recorded after exposing a clean Mo(110) to ethylene at 80 K, can be assigned to an acetylene surface intermediate [26]. This observation clearly indicates that early transition metals, such as Mo(110), are so reactive that they cause the decomposition of the C–H bonds

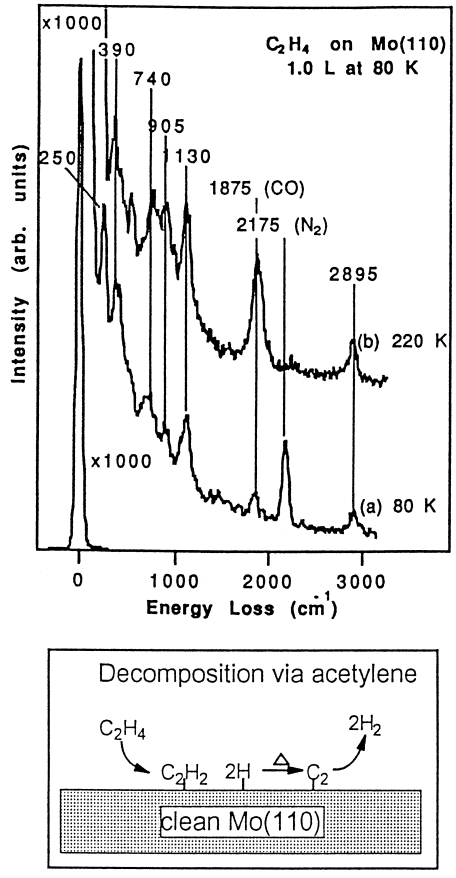

Fig. 2. HREELS spectra following the decomposition of ethylene on a clean Mo(110) surface. The peaks labeled as CO and N_2 are from the adsorption of background contaminants in the UHV systems; the amount of surface CO and N_2 is less than 0.05 monolayer.

of ethylene at temperatures as low as 80 K. As indicated in the reaction scheme in Fig. 2, additional HREELS and TPD studies indicate that the acetylene surface intermediate decomposes to produce atomic carbon and molecular hydrogen at higher temperatures [26].

On the other hand, Fig. 3 shows that the reaction pathway of ethylene on the p(4 × 4)-C/Mo(110) surface is qualitatively different. The HREELS spectrum recorded at 80 K can be assigned to the molecularly adsorbed di-σ ethylene species at 80 K [26], indicating that the p(4 × 4)-C/Mo(110) surface is less reactive towards the decomposition of ethylene. More im-

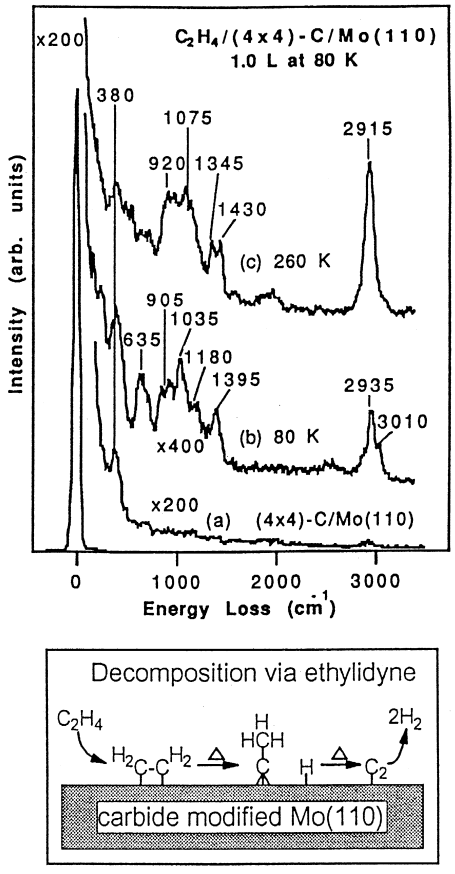

Fig. 3. HREELS results following the decomposition of ethylene on a p(4×4)-C/Mo(110) surface. The formation of the ethylidyne species is detected by the characteristic vibrational spectrum at 260 K.

portantly, the HREELS spectrum, recorded after heating the surface to 260 K, reveals the formation of the characteristic ethylidyne (CCH_3) species [26]. As stated earlier, such a decomposition pathway is very similar to those typically observed on the close-packed faces of Pt-group metals [47–53]. The HREELS results in Fig. 3 demonstrate the similar surface reactivities between p(4 × 4)-C/Mo(110) and Pt-group metals; these results also indicate that the decomposition of ethylene can be used as a characteristic probing reaction to follow the conversion of surface reactivities of early transition metals [11,26], via the formation of a carbide overlayer, to those of Pt-group metals.

3.2. Production of 2-butyne from cis- and trans-2-butenes

Because of the presence of both α-(C–H) and β-(C–H) bonds in *cis*- and *trans*-2-butenes, the decomposition pathways of these two molecules can be used as probing reactions for the investigation of the selective activation of α- and β-CH bonds. For example, if the metal surface is very selective in the dissociation of the α-CH bonds, both 2-butene molecules would decompose to produce 2-butyne. In an early HREELS study, Avery and Sheppard [54] found that the Pt(111) surface was very selective for α-CH bond scission in both *cis*- and *trans*-2-butenes, leading to the formation of 2-butyne as a common surface intermediate at $\sim$ 300 K.

The decomposition mechanisms of *cis*- and *trans*-2-butenes are different on a Mo(110) surface [30]. For example, the clean Mo(110) surface induces the dissociation of both α- and

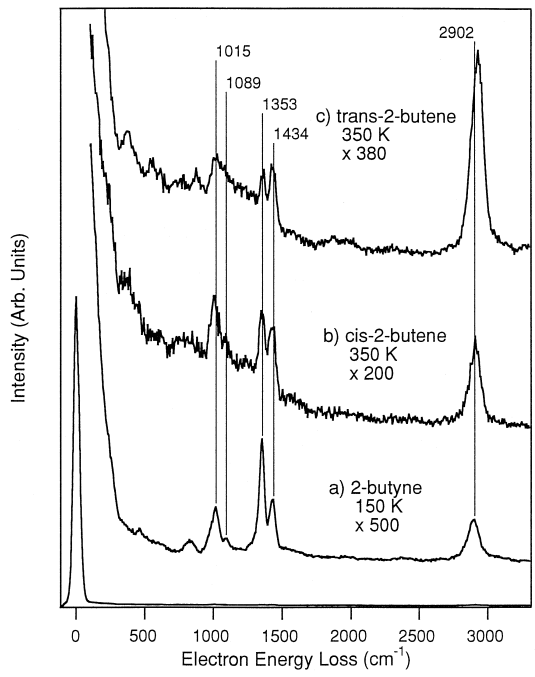

Fig. 4. Comparison of a vibrational spectrum of chemisorbed 2-butyne (a) with reaction intermediates from *cis*-2-butene (b) and *trans*-2-butene (c). The 2-butenes were adsorbed on the p(4×4)-C/Mo(110) surface at 80 K and the adsorbed layers were subsequently heated to 350 K.

β-CH bonds of *trans*-2-butene, leading to the formation of complex C_4H_x surface intermediates. On the other hand, the formation of the carbide overlayer modifies the reactivity of Mo(110), making the p(4 × 4)-C/Mo(110) surface very selective for the activation of the α-CH bonds in a similar fashion as the Pt(111) surface. Fig. 4 shows a comparison of HREELS spectra after the decomposition of *cis*- and *trans*-2-butenes on p(4 × 4)-C/Mo(110) by heating the adsorbed layers to 350 K [30]. The number of vibrational modes and their frequencies of both intermediates are remarkably similar to those of molecularly adsorbed 2-butyne on the same surface, confirming the formation of 2-butyne via the selective activation of the α-CH bonds in both 2-butenes. The differences in the relative intensities are most likely due to different molecular orientations of the 2-butyne molecules with respect to the surface [30].

Fig. 4 also reveals that the vibrational spectrum of 2-butyne is relatively simple compared to most other hydrocarbon molecules or fragments on surfaces [44–46]. This is obviously due to the symmetric structure of 2-butyne, and due to the fact that 2-butyne has only one type of CH bond. The easily identifiable vibrational spectrum of 2-butyne therefore makes the decomposition of *cis*- and *trans*-2-butenes a simple probing reaction to study the reactivities of carbide-modified surfaces.

3.3. Evolution of benzene from dehydrogenation of cyclohexene

Another probing reaction, which only requires simple experimental techniques such as TPD and AES, is the evolution of gas phase benzene from the dehydrogenation of cyclohexene. The two major decomposition pathways of cyclohexene can be expressed by the following net reactions:

$$c - C_6H_{10(a)} \rightarrow 6C_{(a)} + 5H_2(g) \quad (1)$$

$$c - C_6H_{10(a)} \rightarrow C_6H_6(g) + 2H_2(g) \quad (2)$$

where Eq. (1) represents the complete decomposition of all C–H and C–C bonds of cyclohexene to form atomic carbon and hydrogen, and Eq. (2) shows the partial dehydrogenation of cyclohexene to produce benzene and hydrogen. Rodriguez and Campbell [55] and Henn et al.

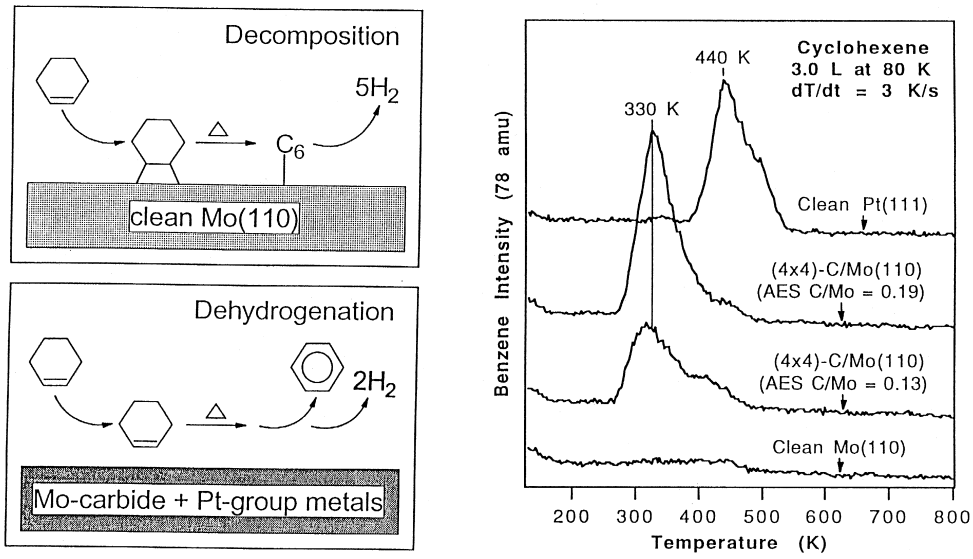

Fig. 5. Comparison of TPD results following the evolution of gas phase benzene from the dehydrogenation of cyclohexene on the Mo(110), p(4 × 4)-C/Mo(110) and Pt(111) surfaces.

[56] have demonstrated that the relative contributions from the two net reactions, defined as the benzene yield, can be readily determined by carefully measuring the TPD peak areas of H_2 and benzene and by measuring the AES C(KLL) intensity after the decomposition. It is well established in the literature that a relatively high benzene yield is typically observed following the reaction of cyclohexene on clean Pt(111) [55,56] or alloyed Pt(111) surfaces [49,57–59].

Fig. 5 shows a comparison of TPD spectra of benzene, produced by the dehydrogenation of cyclohexene, from Mo(110), C/Mo(110) and Pt(111) surfaces [27]. As indicated in the reaction scheme in the left panel of Fig. 5, the clean Mo(110) surface reacts very strongly with cyclohexene, leading to the complete decomposition of all C–H and C–C bonds. As a result, benzene is not detected as the gas phase product. In contrast, benzene is produced on the two (4×4)-C/Mo(110) surfaces, with the surface of a higher C/Mo atomic ratio producing a higher benzene yield. The TPD results in Fig. 5 clearly indicate that the formation of a carbide overlayer converts the major reaction pathway of cyclohexene from complete decomposition on clean Mo(110) to selective dehydrogenation on $p(4 \times 4)$-C/Mo(110) to produce benzene, which is also the dominant reaction mechanism on Pt(111). The difference in the desorption temperatures of benzene from the two surfaces is due to the fact that the production of gas phase benzene is reaction-limited on $p(4 \times 4)$-C/Mo(110) [28,29] but desorption-limited on Pt(111) [56]; the conversion of chemisorbed cyclohexene to benzene is completed at ~ 330 K on both surfaces. Furthermore, a detailed TPD and AES comparison of the $p(4 \times 4)$-C/Mo(110) and Pt(111) surfaces reveals a similar benzene yield for the two surfaces [27]. These results demonstrate that, using simple techniques such as TPD and AES, the dehydrogenation of cyclohexene can be used as a characteristic reaction to probe the conversion of surface reactivities of early transition metals to those of Pt-group metals.

4. The effect of underlying electronic and structural properties

In Section 3, we demonstrated that the formation of a carbide overlayer converts the reactivities of early transition metals to those of Pt-group metals, and that the reactions of ethylene, 2-butenes, and cyclohexene can be used as characteristic probing reactions to follow such a conversion. In this section, we will demonstrate that whether the Pt-like properties can be achieved depends strongly on the local structural and electronic properties of the carbide overlayers. Specifically, the reactivities are directly related to the binding sites of carbon, the chemical nature of carbon, and electronic properties that are related to the metal–carbon bonds.

4.1. The effect of carbon binding sites

Fig. 6 shows the different reactivities of the surface and interstitial carbides by following the

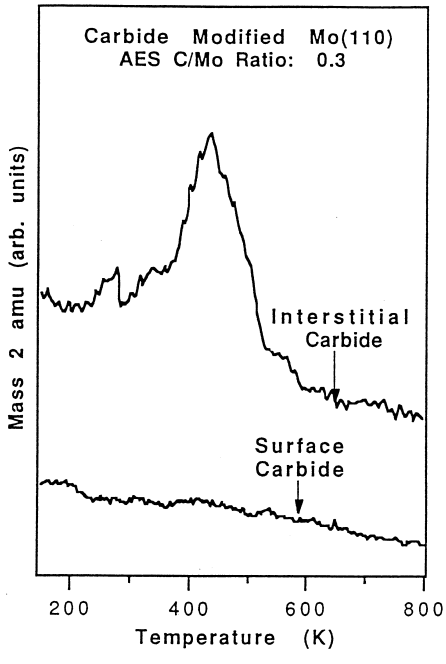

Fig. 6. Comparison of TPD data of H_2, produced by the decomposition of ethylene, on a Mo(110) surface that is modified by surface carbide and interstitial carbide overlayers. See text for a more detailed explanation of the differences between the carbide overlayers.

desorption of H_2, produced by the decomposition of ethylene, on the two surfaces [25]. As discussed earlier in Fig. 1, the combined NEXAFS, XPS and AES results indicate that the carbide overlayer on Mo(110), produced by exposing to high exposures of ethylene at 600 K, is characterized by carbon atoms occupying the surface sites [25]. By annealing the carbide overlayer to temperatures above 1150 K, the surface carbon atoms undergo an inward diffusion to occupy the interstitial sites, producing a sharp p(4 × 4)-C/Mo(110) LEED pattern [25]. It is important to point out that the same p(4 × 4) LEED pattern is also detected on the interstitial α-Mo_2C(0001) single crystal surface by Oyama (private comm.). For ease of comparison, we will refer to the 600 K C/Mo(110) and the annealed (4 × 4)-C/Mo(110) as surface and interstitial carbides, respectively.

As shown in Fig. 6, both carbide surfaces were characterized by an AES C(KLL)/Mo(MNN) ratio of 0.3; furthermore, carbon atoms on both surfaces were carbidic in nature as determined by both XPS and NEXAFS [25]. Ethylene reacts with the interstitial (4 × 4)-C/Mo(110) surface to produce ethylidyne, which further decomposes at higher temperatures to evolve H_2, as detected in the upper TPD spectrum in Fig. 6. In contrast, the H_2 desorption peak is absent on the surface carbide overlayer in the bottom TPD spectrum, indicating that the Mo(110) surface modified by the surface carbide is completely inert towards the decomposition of ethylene. This comparison clearly indicates the critical importance of the location of carbon atoms in determining the reactivities of carbide-modified surfaces.

4.2. The effect of carbon chemical nature

The chemical nature of carbon atoms can vary from carbidic to graphitic, particularly on late transition metal surfaces. To demonstrate the different modification effect of carbidic and graphitic carbon, Fig. 7 shows a comparison of TPD measurements of benzene formation from

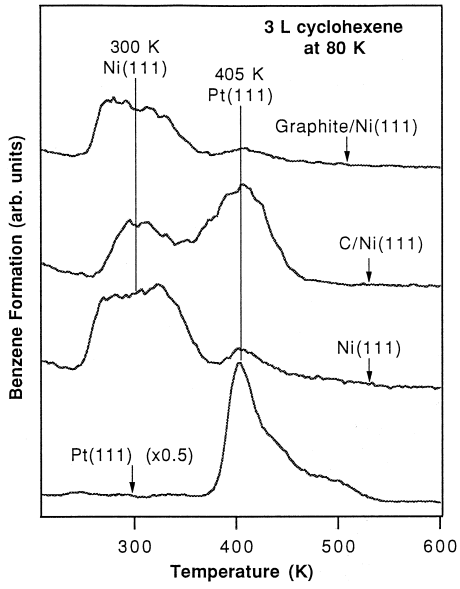

Fig. 7. TPD results following the evolution of benzene from the dehydrogenation of cyclohexene on clean Pt(111) and on Ni(111) thin films epitaxially grown on the Pt(111) substrate. The Pt(111) substrate was completely buried by the Ni overlayer in both clean and carbon-modified Ni(111)/Pt(111) surface as verified by the absence of any Pt Auger transitions in the AES measurements.

the dehydrogenation of cyclohexene on carbide-modified and graphite-modified Ni(111) surfaces [60]. The Ni(111) thin film was grown epitaxially by depositing Ni on a Pt(111) surface at 600 K. The carbide-modified surface was prepared by exposing the Ni(111)/Pt(111) substrate to ethylene at 600 K; the carbidic carbon on Ni(111) can be completely converted to graphite by heating to ≥ 750 K. The carbidic or graphitic nature of the carbon atoms on the Ni(111)/Pt(111) surface was confirmed by XPS [60].

For comparison, Fig. 7 also includes the production of gas phase benzene from the dehydrogenation of cyclohexene on Pt(111) and on the epitaxially grown film of Ni(111)/Pt(111). Benzene desorption, which occurs on both metal surfaces, is detected as an asymmetric peak at 405 K on Pt(111) and as a broad peak centered at ~300 K on Ni(111). After modifying the Ni(111) surface by carbide formation, an intense benzene desorption peak is observed on

the C/Ni(111) surface at 405 K, which coincides with the desorption temperature on the Pt(111) surface. However, this desorption peak almost completely disappears on the graphite-modified Ni(111) surface. A comparison of the graphite-modified Ni(111) surface with clean Ni(111) shows a decrease in the overall TPD peak area of benzene from the former surface, which can be attributed to a reduced number of surface Ni sites due to the presence of graphite on the surface [60]. The most important conclusion from Fig. 7 is that carbidic and graphitic carbon atoms modify the surface reactivities of Ni(111) in a qualitatively different manner.

4.3. The effect of parent metals

The reactivities of carbide-modified surfaces are often different from one transition metal to another. For example, carbide-modified V(110) and Mo(110) surfaces demonstrate significant differences in the activation of C–H bonds of alkanes [6,14]. We attempt to attribute the different reactivities of these two carbide-modified overlayers to their differences in the electronic properties, such as the degree of ionicity in the metal–carbon bonds and in the p-projected density of states (DOS) in vanadium and molybdenum carbides.

The relative ionic and covalent contributions to the metal–carbon bonds, which is determined by the degree of charge transfer between metal and carbon atoms, can vary from one metal to another. In principle, the direction and the amount of charge transfer in the metal–carbon bonds can be estimated from the oxidation state of the metal, which can be measured experimentally using NEXAFS [61–63]. Fig. 8 shows a comparison of NEXAFS investigations of the oxidation states of carbide-modified V(110) and Mo(110) surfaces. The left panel of Fig. 8 shows the peak positions of the vanadium L_{III} and L_{II} NEXAFS features as a function of oxidation state. The vanadium L_{III} and L_{II} transitions are related to the electronic excitations from the $2p_{3/2}$ and $2p_{1/2}$ to 3d orbitals, respectively [62,63], and their peak positions change almost linearly as a function of the vanadium oxidation state. By comparing the V L_{III} and L_{II} peak positions of a thick vanadium carbide overlayer to those of clean V(110) and several standard compounds, including V_2O_3, V_2O_4 and V_2O_5, the oxidation state of vanadium in VC can be estimated to be $V^{1.2\pm0.2}$ [12]. This observation indicates that the direction of charge transfer is from vanadium to carbon and the amount of charge transfer is approximately 1.2 $\pm$ 0.2 electrons per vanadium, clearly indicating

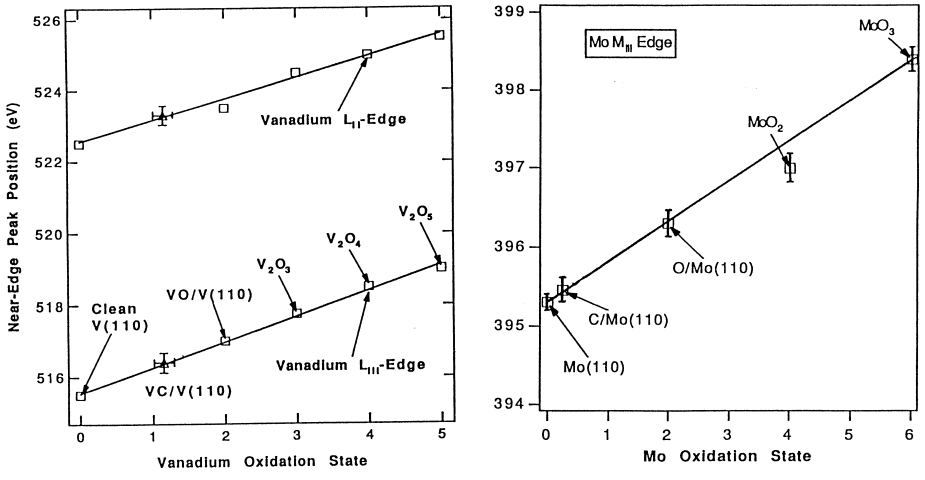

Fig. 8. Comparison of V L-edge (left panel) and Mo M-edge (right panel) NEXAFS peak positions as a function of oxidation state. These measurements provide information regarding the degree of charge transfer between carbon and metal atoms.

a significant amount of ionic contribution in the vanadium–carbon bond [12].

For comparison, the right panel of Fig. 8 shows similar NEXAFS measurements for a carbide overlayer on Mo(110). The peak position of the Mo M_{III} feature, which is related to an electronic transition from Mo $3p_{3/2}$ to 4d orbitals, is shown as a function of Mo oxidation state. Based on the M_{III} peak position, the oxidation state of Mo in the carbide overlayer is approximately $Mo^{0.2 \pm 0.2}$, indicating that the ionic contribution in molybdenum carbide is significantly smaller than that in vanadium carbide.riparian

The different electronic properties of vanadium and molybdenum carbides are also detected in the NEXAFS measurements of the C K-edge features. The C K-edge transitions involve the excitation of C 1s electrons to the partially-occupied or unoccupied molecular orbitals of carbides; the spectral shape of the C K-edge features is directly related to the p-projected density of states (DOS) in transition metal carbides [61,64–66]. The left panel of Fig. 9 shows the C K-edge NEXAFS spectra of vanadium and molybdenum carbides. For comparison, the C K-edge spectrum of graphite is also included. Unlike graphite [67], the C K-edge features of carbides are characterized by two relatively sharp resonances at ≤ 290 eV, which are due to the transitions of C 1s electrons to the p–d(t_{2g}) and p–d(e_g) hybridized orbitals of carbides, respectively [61,64,65]. In addition, there is also a broad feature at ~ 295 eV, which is related to the excitation of C 1s electrons to an unoccupied orbital that involves contributions from 2p and 3p orbitals of carbon and the d and s states of the parent metal [61,64,65]. Fig. 9 also shows that the overall spectral shape of the C K-edge features is significantly different for vanadium and molybdenum carbides, indicating different characteristics in the p-projected DOS of the two carbides.

Finally, for comparison, XPS measurements of vanadium and molybdenum carbides and graphite are shown in the right panel of Fig. 9. Although XPS measurements are capable of differentiating between the carbidic and graphitic nature of the carbon atoms based on the characteristic C(1s) binding energies, they do not reveal the differences in the band structures between vanadium and molybdenum carbides as observed in the NEXAFS measurements. The NEXAFS technique is clearly supe-

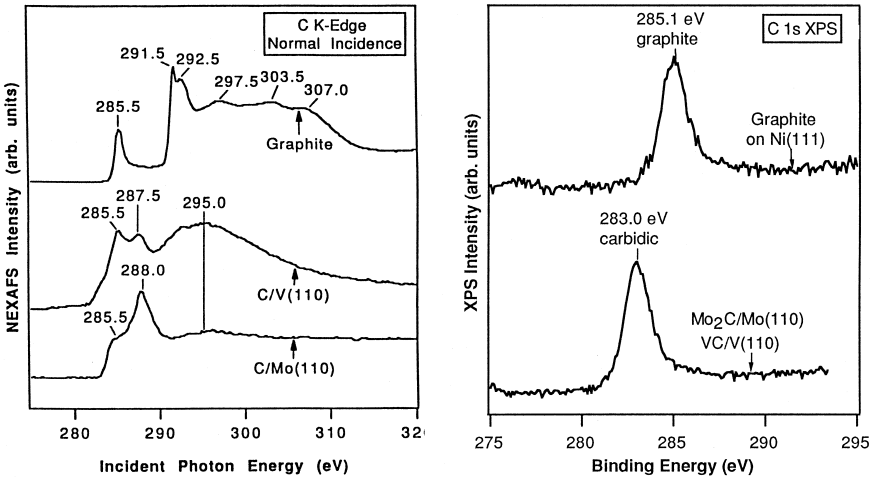

Fig. 9. The C K-edge NEXAFS spectra (left panel) of vanadium carbide, molybdenum carbide and graphite. The NEXAFS spectra of the carbide-modified surfaces were recorded with the incident photon beam normal to the metal surfaces. XPS measurements of the similar materials are compared in the right panel. The XPS binding energy was referenced to the Mo 3d5/2 line at 228.0 eV for clean Mo(110).

rior over the conventional XPS technique in the determination of the nature of the band structures of transition metal carbides. The NEXAFS technique is also very powerful in correlating the structural and electronic properties of model carbide surfaces to those of powder carbide catalysts, as will be discussed in the next section.

5. Comparison of single crystal surfaces with amorphous powder materials

The correlation between well-characterized carbide overlayers and amorphous powder carbide catalysts can be achieved in several ways. One of them involves the comparison of catalytic properties, as demonstrated in the parallel surface science studies of the activation of C4 alkanes on VC/V(110) and the reactor studies of the dehydrogenation of isobutane over vanadium carbide powder catalysts. [3] Another way to compare the electronic, structural, and catalytic properties of single crystal and powder carbide materials can be achieved using NEXAFS [68–70]. For example, NEXAFS spectra of well-characterized carbide overlayers have been used to assist the interpretation of NEXAFS data of bulk powder materials such as Mo_2C [68], of supported carbides such as Mo_2C supported on Al_2O_3 [69], and of more complicated catalyst formulations such as bimetallic oxycarbides such as Mo_2NbC–O [70].

Fig. 10 compares the C K-edge features of a carbide overlayer on Mo(110) to those of powder materials of Mo_2C and Mo_2C–O catalysts. The relatively thick molybdenum carbide overlayer was prepared by multiple cycles of exposing Mo(110) to ethylene at 600 K followed by annealing to above 1150 K [25]. As compared in the left panel of Fig. 10, the peak positions and the relative intensities of the C K-edge features of the molybdenum carbide overlayer and the Mo_2C powder catalysts are in general very similar, except the presence of a small amount of graphite on the powder catalyst as indicated by the relatively weak graphite feature at ~292 eV. On the other hand, although the peak positions of the Mo_2C–O are similar to those of molybdenum carbides, the relative intensity of the C K-edge features are different. These observations suggest that the carbon atoms in Mo_2C–O remain carbidic in nature, but the electronic properties of Mo_2C are modi-

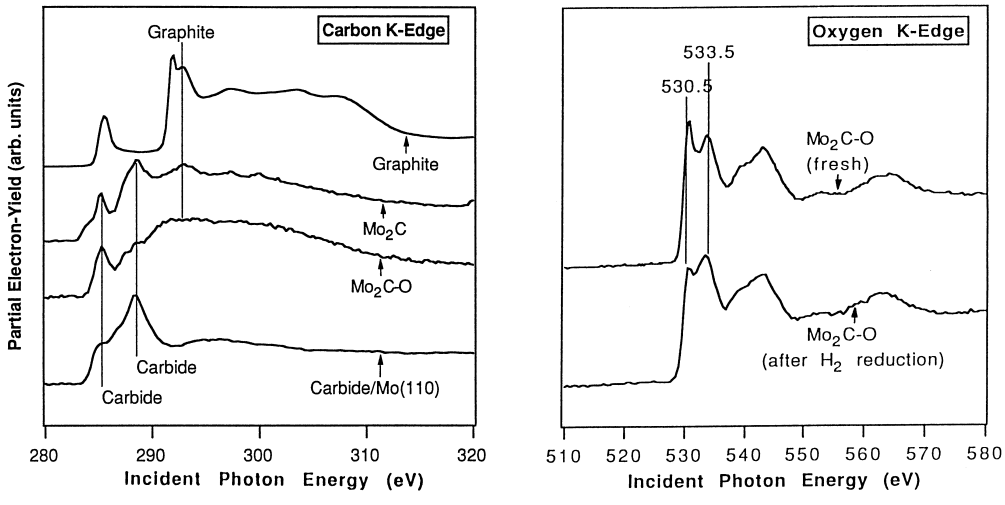

Fig. 10. Comparison of C K-edge features (left panel) of a thick carbide overlayer on Mo(110) with powder materials of Mo_2C and Mo_2C–O. The O K-edge features of Mo_2C–O before and after H_2 reduction (20 Torr H_2 at 727 K for 1 h) are compared in the right panel.

fied by the presence of oxygen. A more detailed understanding of the effect of oxygen modification is of practical importance, because it has been demonstrated by Pham-Huu et al. [71] and Blekkan et al. [72] that the Mo_2C–O catalysts are generally better catalysts than pure Mo_2C in the isomerization of alkane molecules as well as in the activity maintenance.

In addition, for multiple component catalysts such as Mo_2C–O, NEXAFS is a particularly useful tool because it can measure the O K-edge and Mo M_{III}-edge [70] features as well. For example, the local bonding environment of O in Mo_2C–O can be determined by the O K-edge features shown in the right panel of Fig. 10. By comparing the O K-edge features, before and after hydrogen activation, to those of model molybdenum oxide compounds [61], the MoO_x stoichiometry of the H_2-activated Mo_2C–O catalysts can be determined to be $1 > x > 2$.

6. Concluding remarks

The surface science results on model carbide overlayers clearly indicate that the reactivities of transition metals can be modified by the formation of carbide overlayers, with the modified surface reactivities being frequently similar to those of Pt-group metals. In addition, studies on model surfaces provide insightful information on the underlying electronic and structural properties that are controlling the catalytic reactivities of transition metal carbides. Furthermore, recent investigations using NEXAFS also show promise in correlating the findings on single crystal model surfaces to realistic amorphous powder materials.

However, there are still several critical issues that need to be resolved regarding the electronic, structural, and catalytic properties of transition metal carbides. One issue is a need for a better understanding of the physical and chemical properties of the oxycarbide catalysts, which generally show a higher surface area, better catalytic performance, better activity maintenance, and greater stability in air than the pure carbide catalysts. These advantages would certainly make the oxycarbides the preferred catalysts in practical applications. Because the modification of surface reactivities by atomic oxygen is very different from that by carbide, as seen by the well-established differences in reactivities between oxygen-modified Mo(110) [24–30,73,74] and carbide-modified Mo(110) [24–30], a fundamental understanding of the different roles of carbon and oxygen in oxycarbide is of critical importance. More detailed NEXAFS studies in correlating the electronic and catalytic properties of well-characterized oxycarbide surfaces and powder materials would be important experiments. Furthermore, NEXAFS measurements using the fluorescence-yield detection method [61] allow one to carry out in situ studies under non-UHV conditions [75] as well as to differentiate directly surface and bulk compositions [76]. These unique capabilities of the fluorescence-yield NEXAFS method would undoubtedly provide insightful information regarding the catalytic activities of oxycarbides.

Another area of practical catalytic importance is the sulfur and nitrogen tolerance of the carbide catalysts [9,10]. More fundamental studies on the HDS and HDN activities on well-characterized model carbide systems, using surface science spectroscopies, would help to identify the reaction intermediates, and ultimately the HDS and HDN reaction mechanisms, on transition metal carbide catalysts.

Finally, it is important to point out that a closely related class of materials, transition metal nitrides, often demonstrate similar electronic, structural, and catalytic properties as their carbide counterparts. More details regarding the properties of transition metal nitrides can be found in Refs. [1–6].

Acknowledgements

One of us (JE) acknowledges the Exxon Summer Internship during 1995 and 1996.

References

[1] L.E. Toth, Transition Metal Carbides and Nitrides, Academic Press, New York, 1971.
[2] S.T. Oyama, G.L. Haller, Catalysis, Specialist Periodical Reports, G.C. Bond, G. Webb (Eds.), The Chemical Society, Vol. 5, London, 1981, p. 333, and references therein.
[3] S.T. Oyama, The Chemistry of Transition Metal Carbides and Nitrides, Blackie Academic and Professional, Glasgow, 1996.
[4] S.T. Oyama, Catal. Today 15 (1992) 179.
[5] L.I. Johansson, Surf. Sci. Rep. 21 (1995) 177, and references therein.
[6] J.G. Chen, Chem. Rev. 96 (1996) 1477, and references therein.
[7] R.L. Levy, M. Boudart, Science 181 (1973) 547.
[8] F.H. Ribeiro, R.A. Dalla Betta, M. Boudart, J. Baumgartner, E. Iglesia, J. Catal. 130 (1991) 86.
[9] H. Abe, A.T. Bell, Catal. Lett. 18 (1993) 9.
[10] J.C. Schlatter, S.T. Oyama, J.E. Metcalfe III, J.M. Lambert Jr., Ind. Eng. Chem. Res. 27 (1988) 1648.
[11] J.G. Chen, M.D. Weisel, Z.-M. Liu, J.M. White, J. Am. Chem. Soc. 115 (1993) 8875.
[12] J.G. Chen, C.M. Kim, B. Frühberger, B.D. DeVries, M.S. Touvelle, Surf. Sci. 321 (1994) 145.
[13] J.G. Chen, B.D. DeVries, B. Frühberger, C.M. Kim, Z.-M. Liu, J. Vac. Sci. Technol. A 13 (1995) 1600.
[14] J.G. Chen, J. Catal. 154 (1995) 80.
[15] E.I. Ko, R.J. Madix, Surf. Sci. 100 (1980) L449.
[16] E.I. Ko, R.J. Madix, Surf. Sci. 109 (1981) 221.
[17] E.I. Ko, R.J. Madix, Surf. Sci. 112 (1981) 373.
[18] J.L. Grant, T.B. Fryberger, P.C. Stair, Surf. Sci. 159 (1985) 333.
[19] D.S. Kellogg, M.S. Touvelle, P.C. Stair, J. Catal. 120 (1989) 192.
[20] D.G. Kelly, M. Salmeron, G.A. Somorjai, Surf. Sci. 175 (1986) 465.
[21] L.P. Wang, W.T. Tysoe, J. Catal. 128 (1991) 320.
[22] M.B. Young, A.J. Slavin, Surf. Sci. 245 (1991) 56.
[23] J.-W. He, W.K. Kuhn, D.W. Goodman, Surf. Sci. 262 (1992) 351.
[24] B. Frühberger, J.G. Chen, Surf. Sci. 342 (1995) 38.
[25] B. Frühberger, J.G. Chen, J. Eng Jr., B.E. Bent, J. Vac. Sci. Technol. A 14 (1996) 1475.
[26] B. Frühberger, J.G. Chen, J. Am. Chem. Soc. 118 (1996) 11599.
[27] J.G. Chen, B. Frühberger, Surf. Sci. 367 (1996) L102.
[28] J. Eng Jr., B.E. Bent, B. Frühberger, J.G. Chen, J. Phys. Chem. B 101 (1997) 4044.
[29] J. Eng Jr., B.E. Bent, B. Frühberger, J.G. Chen, Langmuir, submitted.
[30] J. Eng Jr., B.E. Bent, B. Frühberger, J.G. Chen, Surf. Sci., submitted.
[31] J.B. Benziger, E.I. Ko, R.J. Madix, J. Catal. 54 (1978) 414.
[32] J.B. Benziger, E.I. Ko, R.J. Madix, J. Catal. 58 (1979) 149.
[33] E.I. Ko, J.B. Benziger, R.J. Madix, J. Catal. 62 (1980) 264.
[34] M.A. Barteau, R.J. Madix, J. Catal. 62 (1980) 329.
[35] J.B. Benziger, E.I. Ko, R.J. Madix, J. Catal. 64 (1980) 132.
[36] C.M. Friend, J.G. Serafin, E.K. Baldwin, P.A. Stevens, R.J. Madix, J. Chem. Phys. 87 (1987) 1847.
[37] K.A. Pearlstine, C.M. Friend, J. Vac. Sci. Technol. A 2 (1984) 1021.
[38] K.A. Pearlstine, C.M. Friend, J. Am. Chem. Soc. 107 (1985) 5898.
[39] K.A. Pearlstine, C.M. Friend, J. Phys. Chem. 90 (1986) 4341.
[40] K.A. Pearlstine, C.M. Friend, J. Phys. Chem. 90 (1986) 4344.
[41] E.K. Baldwin, C.M. Friend, J. Phys. Chem. 91 (1987) 3821.
[42] J.G. Serafin, C.M. Friend, J. Phys. Chem. 92 (1988) 6694.
[43] M.R.A. Blomberg, P.E.M. Siegbahn, M. Svensson, J. Phys. Chem. 96 (1992) 9794.
[44] N. Sheppard, Ann. Rev. Phys. Chem. 39 (1988) 589.
[45] F. Zaera, Chem. Rev. 95 (1995) 2651.
[46] B.E. Bent, Chem. Rev. 96 (1996) 1361.
[47] H. Steininger, H. Ibach, S. Lehwald, Surf. Sci. 117 (1982) 685.
[48] P. Cremer, C. Stanners, J.W. Niemantsverdriet, Y.R. Shen, G.A. Somorjai, Surf. Sci. 328 (1995) 111.
[49] B. Frühberger, J. Eng Jr., J.G. Chen, Catal. Lett., in press.
[50] M.M. Hills, J.E. Parmeter, C.B. Mullins, W.H. Weinberg, J. Am. Chem. Soc. 108 (1986) 3554.
[51] J.A. Gates, L.L. Kosmodel, Surf. Sci. 124 (1983) 68.
[52] P.A.P. Nascente, M.A. Van Hove, G.A. Somorjai, Surf. Sci. 253 (1991) 167.
[53] T.S. Marinova, K.L. Kostov, Surf. Sci. 181 (1987) 573.
[54] N.R. Avery, N. Sheppard, Proc. R. Soc. London A 405 (1986) 27.
[55] J.A. Rodriguez, C.T. Campbell, J. Catal. 115 (1989) 500.
[56] F.C. Henn, A.L. Diaz, M.E. Bussell, M.B. Hugenschmidt, M.E. Domagala, C.T. Campbell, J. Phys. Chem. 96 (1992) 5965, and references therein.
[57] C. Xu, B.E. Koel, Surf. Sci. 304 (1994) 249.
[58] A.V. Teplyakov, B.E. Bent, Surf. Sci., submitted.
[59] A.V. Teplyakov, A.B. Gurevich, B.E. Bent, J.G. Chen, Langmuir, submitted.
[60] J.G. Chen, B. Frühberger, in preparation.
[61] J.G. Chen, Surf. Sci. Reports, submitted.
[62] J.G. Chen, B. Frühberger, M.L. Colaianni, J. Vac. Sci. Technol. A 14 (1996) 1668.
[63] C.M. Kim, B.D. DeVries, B. Frühberger, J.G. Chen, Surf. Sci. 327 (1995) 81.
[64] J. Pflüger, J. Fink, G. Crecelius, K.P. Bohnen, H. Winter, Solid State Commun. 44 (1982) 489.
[65] J. Pflüger, J. Fink, K. Schwarz, Solid State Commun. 55 (1985) 675.
[66] F.M.F. de Groot, J. Electron Spectrosc. Rel. Phen. 67 (1994) 529, and references therein.
[67] J. Stöhr, NEXAFS Spectroscopy, Springer-Verlag, New York, 1991.
[68] R. Kapoor, S.T. Oyama, B. Frühberger, B.D. DeVries, J.G. Chen, Catal. Lett. 34 (1995) 179.
[69] B. Dhandapani, S. Ramanathan, C.C. Yu, S.T. Oyama, B. Frühberger, J.G. Chen, J. Catal., submitted.
[70] C.C. Yu, S. Ramanathan, B. Dhandapani, J.G. Chen, S.T. Oyama, J. Phys. Chem. B 101 (1997) 512.

[71] C. Pham-Huu, M.J. Ledoux, J. Guille, J. Catal. 143 (1993) 249.
[72] E.A. Blekkan, C. Pham-Huu, M.J. Ledoux, J. Guille, Ind. Eng. Chem. Res. 33 (1994) 1657.
[73] J.G. Chen, M.L. Colaianni, W.H. Weinberg, J.T. Yates Jr., Chem. Phys. Lett. 177 (1991) 113.
[74] M.L. Colaianni, J.G. Chen, W.H. Weinberg, J.T. Yates Jr., J. Am. Chem. Soc. 114 (1992) 3735.
[75] J.G. Chen, D.A. Fischer, J.H. Hardenbergh, R.B. Hall, Surf. Sci. 279 (1992) 13.
[76] J.G. Chen, B.D. DeVries, J.T. Lewandowski, R.B. Hall, Catal. Lett. 23 (1994) 25.